Palaeogeography, Palaeoclimatology, Palaeoecology 266 (2008) 28-38

Contents lists available at ScienceDirect

Palaeogeography, Palaeoclimatology, Palaeoecology

journal homepage: www.elsevier.com/locate/palaeo

Precipitation rates and atmospheric heat transport during the Cenomanian greenhouse warming in North America: Estimates from a stable isotope mass-balance model

David F. Ufnar [a,*], Greg A. Ludvigson [b], Luis González [c], Darren R. Gröcke [d]

[a] University of Southern Mississippi, Box 5044, Hattiesburg, MS 39406, USA
[b] Kansas Geological Survey, University of Kansas, Lawrence, Kansas 66047-3726, USA
[c] Department of Geology, University of Kansas, Lawrence, Kansas 66045-7613, USA
[d] Department of Earth Sciences, Durham University, Durham, DH1 3LE, UK

ARTICLE INFO

Article history:
Accepted 25 March 2008

Keywords:
Siderite
Paleoclimatology
Cretaceous
Oxygen isotopes
Precipitation

ABSTRACT

Stable isotope mass-balance modeling results of meteoric $\delta^{18}O$ values from the Cenomanian Stage of the Cretaceous Western Interior Basin (KWIB) suggest that precipitation and evaporation fluxes were greater than that of the present and significantly different from simulations of Albian KWIB paleohydrology. Sphaerosiderite meteoric $\delta^{18}O$ values have been compiled from the Lower Tuscaloosa Formation of southwestern Mississippi (25°N paleolatitude), The Dakota Formation Rose Creek Pit, Fairbury Nebraska (35°N) and the Dunvegan Formation of eastern British Columbia (55°N paleolatitude). These paleosol siderite $\delta^{18}O$ values define a paleolatitudinal gradient ranging from −4.2‰ VPDB at 25°N to −12.5‰ VPDB at 55°N. This trend is significantly steeper and more depleted than a modern theoretical siderite gradient (25°N: −1.7‰; 65°N: −5.6‰ VPDB), and a Holocene meteoric calcite trend (27°N: −3.6‰; 67°N: −7.4‰ VPDB). The Cenomanian gradient is also comparatively steeper than the Albian trend determined for the KWIB in the mid- to high latitudes. The steep latitudinal trend in meteoric $\delta^{18}O$ values may be the result of increased precipitation and evaporation fluxes (amount effects) under a more vigorous greenhouse-world hydrologic cycle. A stable-isotope mass-balance model has been used to generate estimates of precipitation and evaporation fluxes and precipitation rates. Estimates of Cenomanian precipitation rates based upon the mass-balance modeling of the KWIB range from 1400 mm/yr at 25°N paleolatitude to 3600 mm/yr at 45°N paleolatitude. The precipitation–evaporation (*P–E*) flux values were used to delineate zones of moisture surplus and moisture deficit. Comparisons between Cenomanian *P–E* and modern theoretical siderite, and Holocene calcite latitudinal trends shows an amplification of low-latitude moisture deficits between 5–25°N paleolatitude and moisture surpluses between 40–60°N paleolatitude. The low-latitude moisture deficits correlate with a mean annual average heat loss of 48 W/m^2 at 10°N paleolatitude (present, 8 W/m^2 at 15°N). The increased precipitation flux and moisture surplus in the mid-latitudes corresponds to a mean average annual heat gain of 180 W/m^2 at 50°N paleolatitude (present, 17 W/m^2 at 50°N). The Cenomanian low-latitude moisture deficit is similar to that of the Albian, however the mid-latitude (40–60°N) precipitation flux values and precipitation rates are significantly higher (Albian: 2200 mm/yr at 45°N; Cenomanian: 3600 mm/yr at 45°N). Furthermore, the heat transferred to the atmosphere via latent heat of condensation was approximately 10.6× that of the present at 50°N. The intensified hydrologic cycle of the mid-Cretaceous greenhouse warming may have played a significant role in the poleward transfer of heat and more equable global conditions. Paleoclimatological reconstructions from multiple time periods during the mid-Cretaceous will aid in a better understanding of the dynamics of the hydrologic cycle and latent heat flux during greenhouse world conditions.

Published by Elsevier B.V.

1. Introduction

1.1. Purpose

The purpose of this study is to show that siderite nodules in paleosols of the Cenomanian Lower Tuscaloosa Formation (LTF), Dakota Formation, and the Dunvegan Formation have oxygen isotopic

* Corresponding author.
E-mail address: david.ufnar@usm.edu (D.F. Ufnar).

0031-0182/$ – see front matter. Published by Elsevier B.V.
doi:10.1016/j.palaeo.2008.03.033

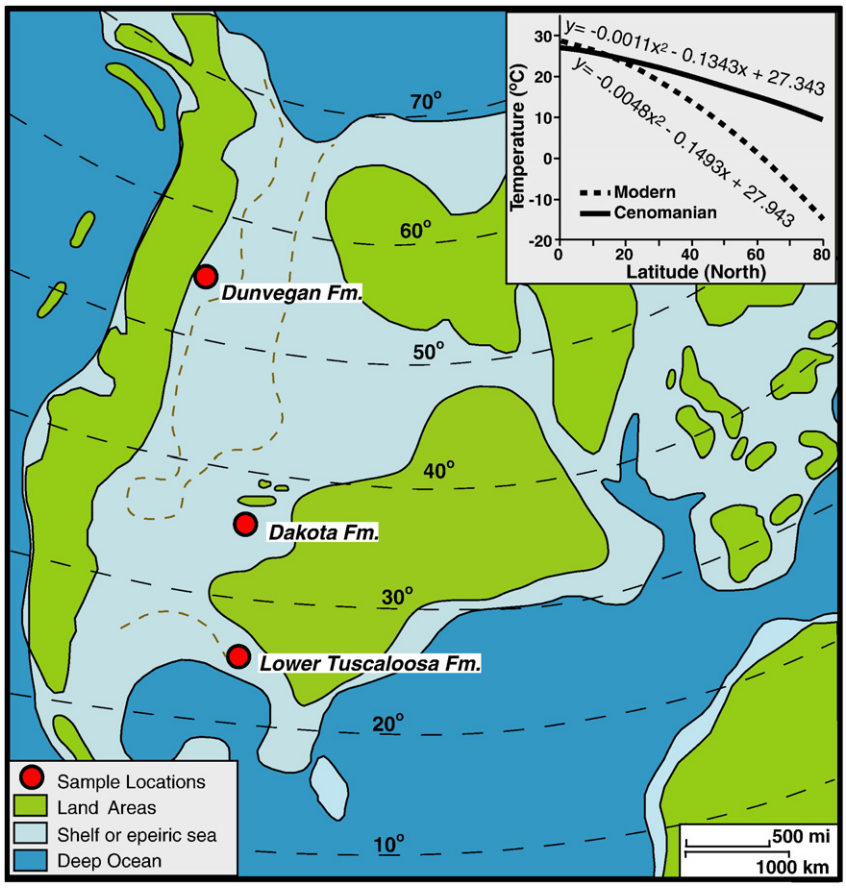

Fig. 1. The map illustrates a paleogeographic reconstruction of the North American continent during Cenomanian–Turonian time. The gradients in the upper right illustrate the temperature gradients and polynomial equations used in the mass-balance modeling experiments (map modified from Witzke, 2003).

values that are a proxy record for low-altitude, coastal plain rainfall $\delta^{18}O$ values during the mid-Cretaceous greenhouse warming (Fig. 1). The new stable isotopic data has been used to reconstruct a latitudinal trend in Cenomanian Stage precipitation isotopic values and model estimates for Cretaceous Western Interior Basin (KWIB) precipitation rates and latent heat flux values during the Cenomanian Stage.

1.2. Geologic significance

Quantifying global transfers of sensible heat by the oceans (Covey and Barron, 1988; Crowley, 1991; Barron et al., 1995; Sloan et al., 1995) and latent heat by the atmosphere are necessary to explain warmer polar temperatures (Parrish and Spicer, 1988a,b) during greenhouse periods of Earth history (Schneider et al., 1985; Huber et al., 1995; Upchurch et al., 1999). Increased global temperatures increase the saturation vapor pressure of the troposphere, and modify latent heat transfer from low to high latitudes (Hay and DeConto, 1999). Furthermore, as water vapor is a greenhouse gas, the increased vapor content of the lower atmosphere enhances the "greenhouse effect" (Rind and Chandler, 1991). Elevated atmospheric pCO_2 levels from large igneous province eruptions (Larson, 1991; Tarduno et al., 1998), and the presence of continental seaways (Poulsen et al., 1999) may have reduced regional thermal gradients by as much as 15 °C. Latent heat flux (LHF) through the atmosphere may also contribute significantly to greenhouse-world heat transfer (Schmidt and Mysak, 1996; DeConto et al., 1999; Hay and DeConto, 1999).

Empirical isotopic data from paleosol siderite nodules (sphaerosiderites) in the KWIB (Fig. 2; Ludvigson et al., 1998; White et al.,

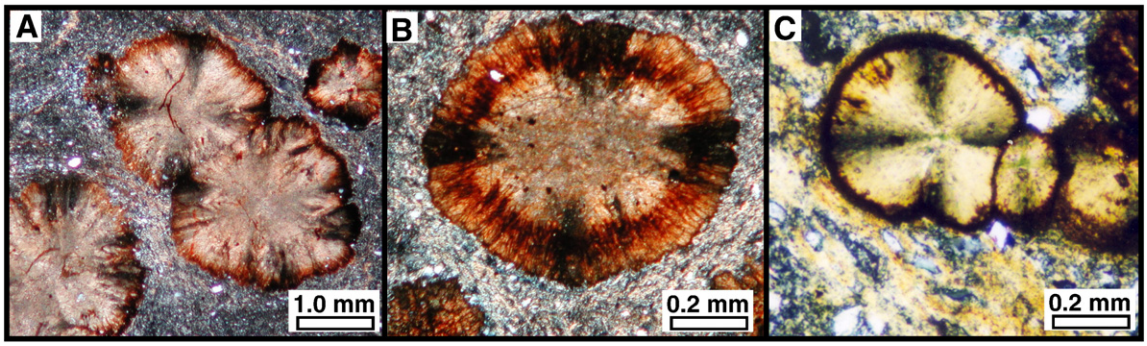

Fig. 2. The photomicrographs illustrate representative sphaerosiderites from the (A) Lower Tuscaloosa Formation, Harrell Smith Core #1–11, Mississippi, (B) Dakota Formation, Rose Creek Pit, Nebraska, and (C) The Dunvegan Formation, Kaskatinaw Gorge, British Columbia.

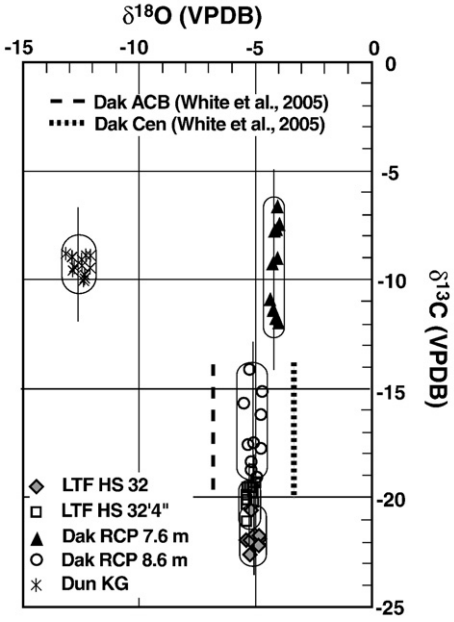

Fig. 3. The plot shows the range of $\delta^{18}O$ vs. $\delta^{13}C$ values for sphaerosiderites obtained from the Lower Tuscaloosa Formation (LTF HS), #1–11 Harrell Smith Core (2936.6–2936.7 m depth intervals), the Dakota Formation Rose Creek Pit (Dak RCP) 7.6 and 8.6 m intervals, and the Dunvegan Formation Kaskatinaw River Gorge (Dun KG, sequence boundary F, position marked "E" in Fig. 7 of McCarthy et al., 1999b). The vertical lines through the data points illustrate the average $\delta^{18}O$ value with the range of $\delta^{13}C$ values defining the MSL. The $\delta^{13}C$ values are more variable than the $\delta^{18}O$ values and are used to show that the MSLs are early-diagenetic trends resulting from siderite precipitation in a stable groundwater system. Additional MSLs for the Dakota Formation Cenomanian (Cen) and Albian–Cenomanian Boundary (ACB) are illustrated from White et al. (2005).

2000a,b; Ufnar et al., 2001; White et al., 2001; Ufnar et al., 2002, 2004a,b,c, 2005a,b,c; White et al., 2005) are used to quantify precipitation and evaporation fluxes in the hydrologic cycle (Ludvigson et al., 1998, White et al., 2001; Ufnar et al., 2002). The use of sphaerosiderite $\delta^{18}O$ values as a paleohydrologic proxy record is made possible by the recognition of Meteoric Sphaerosiderite Lines — MSLs (Ludvigson et al., 1998). MSLs are early-diagenetic trends defined by sphaerosiderite isotopic values with invariant $\delta^{18}O$ values, and highly variable $\delta^{13}C$ values. The MSLs are analogous to meteoric calcite lines (Lohmann, 1988). The invariant $\delta^{18}O$ values reflect precipitation in a ground water system with stable $\delta^{18}O$ values, and uniform temperature (Ludvigson et al., 1998; White et al., 2001; Ufnar et al., 2002).

Mass-balance modeling of the hydrologic cycle (Ufnar et al., 2002) during the Albian Stage suggests enhanced LHF during the mid-Cretaceous greenhouse warming (Ufnar et al., 2004c). Quantifying LHF is essential to understanding reduced equator-to-pole temperature gradients.

1.3. The mid-Cretaceous hydrologic cycle

The $\delta^{18}O$ values of sphaerosiderites from paleosol horizons (Fig. 3) define a latitudinal gradient in meteoric $\delta^{18}O$ values that is steeper and more depleted than modern analogues (Fig. 4). The Cenomanian $\delta^{18}O$ latitudinal trend is also 7.5 (at 25°N lat.) to 9.0‰ (at 55°N lat.) lighter than the trend predicted using modern empirical temperature — $\delta^{18}O$ relationships (Dansgaard, 1964; Rozanski et al., 1993). The sphaerosiderite proxy data have been used to constrain a mass-balance model (modified from Ufnar et al., 2002) of isotopic compositions of precipitation to quantify changes in the Cenomanian hydrologic cycle. The model results show increased precipitation and evaporation fluxes, and accounts for the steeper meteoric $\delta^{18}O$ gradient with some significant differences from the results generated for the Albian. The intensified hydrologic cycle provides an effective mechanism for exporting large amounts of tropical heat to higher latitudes, and the mass-balance model results have been used to generate quantitative estimates of LHF during the Cenomanian greenhouse warming.

These data provide quantitative estimates of paleoprecipitation and LHF for the Cenomanian stage of the mid-Cretaceous. It is essential to refine the empirically-based estimates of LHF during greenhouse periods because general circulation models (GCM) of the mid-Cretaceous tend to underestimate the export of tropical heat to higher latitudes through the atmosphere.

2. Methods

2.1. Sphaerosiderite-bearing paleosols

The Cenomanian-aged (Mancini et al., 1987) sphaerosiderite-bearing paleosols of the Lower Tuscaloosa Formation were obtained from the Kern Brooks Oil Operations #1–11 Harrell Smith Core from Jefferson County, Mississippi (Cameron et al., 1992). The Dakota Formation samples were obtained from the fluvial/estuarine deposits of the Rose Creek Pit (RCP) near Fairbury, Nebraska (Gröcke et al., 2006). The sphaerosiderite-bearing paleosols analysed from the Dunvegan Formation were obtained from the Type 5 paleosol pedocomplex marking position "E" in the east section of the Kaskatinaw River (New Bridge) section described by McCarthy and Plint (1999).

2.2. Stable isotopes

The stable isotope analyses from the Lower Tuscaloosa Formation were conducted at the University of Kansas Stable Isotope Research Lab directed by Luis A. González. The Dakota Formation siderite analyses were conducted by Lora Wingate at the University of Michigan Stable Isotope Laboratory. The Dunvegan Formation siderite analyses were produced by the authors at the Paul H. Nelson Stable Isotope Laboratory at the University of Iowa (Ufnar et al., 1999). The powdered samples were roasted in vacuo at 380 °C to remove volatile contaminants. Samples were then reacted with anhydrous phosphoric acid at 75 °C in a Kiel III automated carbonate reaction device coupled to the inlet of a Finnigan MAT 252 or 253 isotope ratio mass spectrometer. All isotope ratios are reported relative to the Vienna PeeDee Belemnite (VPDB) standard, with analytical precision of better than ±0.1‰ $\delta^{13}C$ and $\delta^{18}O$ values. The siderite data were corrected

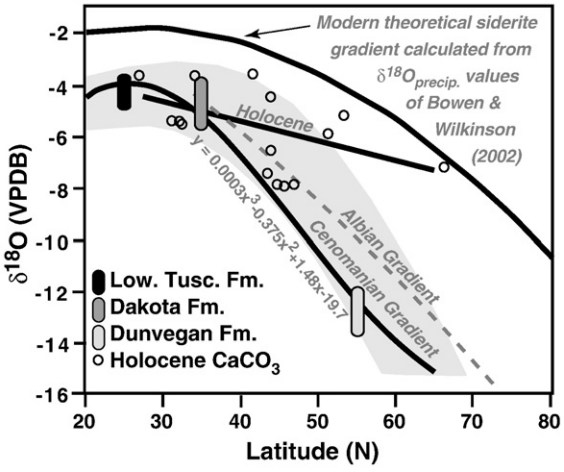

Fig. 4. The gradients illustrated on the graph are the latitudinal trends in Cenomanian sphaerosiderite $\delta^{18}O$ values, Albian sphaerosiderite $\delta^{18}O$ values, modern Theoretical siderite $\delta^{18}O$ values based upon the latitudinal trend in meteoric $\delta^{18}O$ values from Bowen and Wilkinson (2002), and a Holocene trend in meteoric calcite $\delta^{18}O$ values from a broad range of latitudes (see Table 1. for sources).

with the experimentally determined temperature-dependent oxygen isotope fractionation factor (Carothers et al., 1988).

2.3. Mass-balance model

The sphaerosiderite isotope values from the Cenomanian paleosols described here have been used to generate a latitudinal gradient in meteoric $\delta^{18}O$ values between 25° and 55°N paleolatitude. The Cenomanian trend in siderite $\delta^{18}O$ values is compared to three modern analogues. The modern trends in meteoric $\delta^{18}O$ values were used to calibrate the stable isotope mass-balance model. The first trend used is a theoretical siderite $\delta^{18}O$ gradient that was calculated from the International Atomic Energy Agency, World Meteorological Organization (IAEA/WMO) mean annual $\delta^{18}O$ values of precipitation from low-altitude monitoring stations around the world (Rozanski et al., 1993). This is the same gradient that was generated for the Albian mass-balance modeling of Ufnar et al. (2002). The second modern trend was adopted from the $\delta^{18}O$ of precipitation gradient modeled by Bowen and Wilkinson (2002). Their polynomial equation which represents the latitudinal gradient in precipitation values was coupled with the modern mean annual temperature gradient and the fractionation factor of Carothers et al. (1988) to calculate a theoretical modern siderite $\delta^{18}O$ gradient. Bowen and Wilkinson's (2002) equation has an elevation factor and the value of 10 m was used to represent low elevation modern siderite values. The third modern trend was compiled from Holocene speleothem and meteoric calcite cement values over a broad range of latitudes (22°–65° latitude; Table 1). The Holocene calcite values were used to compare recent empirical proxy records for meteoric water $\delta^{18}O$ values to the Cenomanian empirical proxy records in addition to the theoretical modern siderite values.

Detailed descriptions of the stable isotope mass-balance model used for this investigation are provided in Ufnar et al. (2002). The mass-balance model is designed to reproduce a latitudinal trend in siderite $\delta^{18}O$ values and it is controlled by 6 input variables: (1) a latitudinal temperature gradient; (2) a latitudinal trend in relative humidity; (3) a latitudinal trend in meteoric $\delta^{18}O$ values; (4) the mean $\delta^{18}O$ value of ocean water; (5) precipitation flux; and (6) evaporation flux. The model is designed to simulate the changes in meteoric $\delta^{18}O$ values that occur as a theoretical airmass develops in the tropics and progresses towards higher latitudes through Hadley, Farrell, and Polar cell circulation. With each step in its latitudinal traverse, the airmass is losing a fraction of its water vapor through precipitation (precipitation flux) and gaining some moisture back through evapotranspiration (evaporative flux). With each step in latitude, the $\delta^{18}O$ value of the air mass water vapor is recalculated (water vapor fractionation factors of Majoube, 1971) with the mass-balance equation (Ufnar et al., 2002) based upon the input values (Eq. (1)).

$$\delta^{18}O_{a(n)} = \frac{\left[\delta^{18}O_{a(n-1)} \bullet f_{(n-1)} + \left(\delta^{18}O_v \bullet \frac{de}{dt} - \delta^{18}O_r \bullet \frac{dr}{dt}\right)\right]}{\left[f_{(n-1)} - \frac{de}{dt} + \frac{dr}{dt}\right]} \quad (1)$$

$\delta^{18}O_{a(n)}$	composition of water vapor in the air mass.
f	fraction of vapor remaining in the vapor reservoir.
$\delta^{18}O_v$	composition of vapor added via evaporation.
de/dt	vapor fraction added through evaporation (vapor flux).
$\delta^{18}O_r$	composition of precipitation removed from the air mass.
dr/dt	vapor fraction removed through precipitation (precipitation flux).
n	latitude.

The model is dimensionless, thus precipitation and evaporation fluxes are used to add or remove a fraction of vapor from a supply that starts at 0° latitude with an initial value of 1. In executing the model, the latitudinal temperature gradient, meteoric $\delta^{18}O$ gradient; relative humidity gradient; and $\delta^{18}O$ of ocean water are held constant. The precipitation and evaporation fluxes are the variables that are altered through multiple iterations until the model reproduces a gradient in siderite $\delta^{18}O$ values that is identical to the polynomial regression "best-fit" line of the empirical siderite data. The model was first calibrated by using a modern latitudinal trend in mean annual temperatures, $\delta^{18}O$ of precipitation, and 0‰ VSMOW for the $\delta^{18}O$ value of ocean water. For the Holocene meteoric calcite trend, the model was reconfigured to calculate calcite $\delta^{18}O$ values rather than siderite (calcite–water fractionation factor from Faure, 1986). The modeled $\delta^{18}O$ values account for the kinetic effects of humidity using the relationship established by Gonfiantini (1986; see equation 2 in Ufnar et al., 2002).

Upon completing the modern simulations, the input variables were changed for the Cenomanian gradient. The modern temperature gradient was replaced with the temperature gradient of Spicer and Corfield (1992) based upon the fossil vegetation data of Wolfe and Upchurch (1987). The $\delta^{18}O$ value of ocean water was changed to −1‰ VSMOW (Shackleton and Kennett, 1975; Dettman and Lohman, 2000); and the latitudinal trend in meteoric $\delta^{18}O$ values was changed to a gradient that is very similar to the meteoric values calculated from the sphaerosiderites. Using the $\delta^{18}O$ values calculated from the sphaerosiderites presents some circular reasoning; however the alternative is to input completely hypothetical values. Sensitivity tests have shown that the model outputs are sensitive to changes in the continental vapor feedback parameter (Ufnar et al., 2002). Independently-determined meteoric $\delta^{18}O$ values are lacking, thus the meteoric values estimated from the sphaerosiderites are the best analogue until an independent empirical data set can be compiled.

Table 1
Sources of $\delta^{18}O$ values from Holocene meteoric calcites

Latitude	Avg. $\delta^{18}O$ VPDB (age <5 ka)	Location	Source
27.2	−3.6	Caverna Botuverá, Brazil	Wang et al. (2006)
31.5	−5.3	Soreq Cave, Central Israel	Bar-Matthews et al. (2003)
32.1	−5.3	Nahal Qanah cave, Israel	Frumkin et al. (1999)
32.6	−5.5	Peqiin Cave, Northern Israel	Bar-Matthews et al. (2003)
34.3	−3.5	Moondyne Cave, Australia	Treble et al. (2005)
41.7	−3.5	northwest South Island, NZ	Williams et al. (2005)
43.5	−7.4	Cold Water Cave, IA, USA	Denniston et al. (1999a)
44.1	−6.5	Mystery Cave, MN, USA	Denniston et al. (1999b)
44.1	−4.3	Spring Valley, MN, USA	Denniston et al. (1999b)
44.8	−7.8	Crystal Cave, WI, USA	Denniston et al. (1999b)
45.8	−7.9	Postojna Cave,	Horvantinčič et al. (2003)
47.1	−7.8	Ursilor Cave, near Oradea, Romania	Onac et al. (2002)
51.1	−5.8	Atta cave, Attendorn, Germany	Niggemann et al. (2003b)
51.4	−5.8	B7 Cave, Hagen, Germany	Niggemann et al. (2003a)
53.5	−5.1	Stump Cross Caverns, Yorkshire, England	Baker et al. (1997)
66.4	−7.1	Mo i Rana, Norway	Linge et al. (2001)

3. Results

3.1. Paleosol descriptions

3.1.1. Lower Tuscaloosa Formation

The sphaerosiderite-bearing paleosols observed in the Harrell Smith core (3210.6–3211 m) are clay dominated mudstones with <10% very fine-grained quartz sand. The mudstones exhibit a striated birefringence fabric (b-fabric) and common clay coatings and infillings. The clay coatings are characterized by moderate- to well-oriented clay particles characterized by wavy extinction patterns

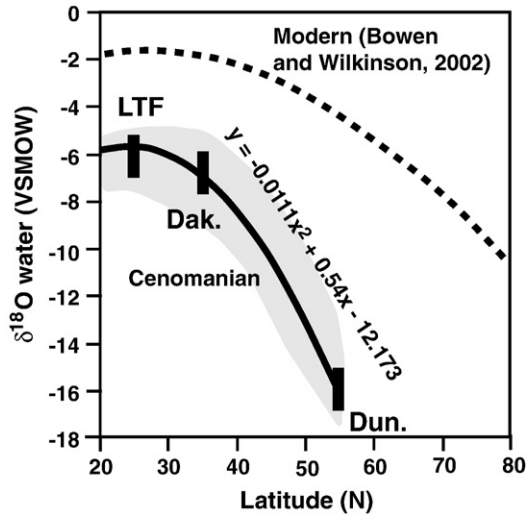

Fig. 5. The graph illustrates the differences in the latitudinal trends in meteoric water $\delta^{18}O$ values for the present (gradient from Bowen and Wilkinson, 2002), and the Cenomanian of the KWIB. The Cenomanian trend is estimated from the paleotemperature estimates of Wolfe and Upchurch (1987) and the Lower Tuscaloosa, Dakota, and Dunvegan Formation sphaerosiderite $\delta^{18}O$ values.

under cross-polarized light (Bullock et al., 1985) and correspond to the sepic plasmic fabrics of Brewer (1964). The clay coatings are generally fragmented, discontinuous, and exhibit gradational contacts with the surrounding matrix. The paleosol groundmass is predominantly grey with 30–50% prominent, coarse, purple-red mottling. The sphaerosiderites range from 1.0 to 1.75 mm in diameter, have radial concentric crystalline microstructures, and have faint to prominent oxidation rings (Fig. 2). The oxidation rings are thicker and more prominent in the red-mottled domains.

3.1.2. Dakota Formation Rose Creek Pit

The Rose Creek Pit claystone paleosols exhibits striated b-fabrics characterized by elongated zones of oriented clay particles that exhibit simultaneous extinction patterns. The matrix contains discontinuous, fragmented and degraded clay coatings. The matrix contains a minor amount of pyrite (0.01–0.02 mm) framboids encased within fine, faint yellow mottles. The sphaerosiderites generally occur as individual nodules up to 1.0 mm in diameter. The nodules have a microcrystalline siderite (micrite-like) core surrounded by bladed, radial-concentric siderite crystallites. The outer terminations of the bladed crystallites are euhedral to eroded and moderately- to strongly impregnated with a red iron oxide stain. Commonly, the sphaerosiderite nodules contain minor inclusions of pyrite (0.01–0.02 mm size framboids) or quartz silt grains.

3.1.3. Dunvegan Formation

The sphaerosiderite-bearing paleosols are characterized by silty- to very fine-grained sandy mudstones with speckled- and striated b-fabrics. The matrix is dominated by domains of prominent, dark red (ferruginous) mottles complexly mixed with domains of light grey-green reduction halos or rhizohaloes (Kraus and Hasiotis, 2006). Clay coatings and infillings are common, and generally occur as discontinuous pore and void coatings with moderate- to well-oriented clay particles. The sphaerosiderite nodules (0.25–0.5 mm diameter) are often observed in linear arrays adjacent to voids, and as pseudomorphs of organic fragments. Internally, the nodules generally exhibit a radial concentric crystalline microstructure and often contain cubic or framboidal pyrite inclusions (generally <0.2 mm in size). Commonly, individual sphaerosiderite nodules are characterized by serrated margins with a prominent, opaque oxidation rim.

3.2. Stable isotope data

3.2.1. Lower Tuscaloosa Formation

The 3210.6 m interval of the Harrell Smith core yielded $\delta^{18}O$ values that ranged from −5.4 to −4.8‰ with an average, MSL value of −5.0± 0.19‰ VPDB (Fig. 3). The $\delta^{13}C$ values ranged from −22.6 to −20.3‰ with an average value of −21.8‰ VPDB. The 3211 m interval yielded $\delta^{18}O$ values that ranged from −5.3 to −4.9‰ and the average, MSL value is −5.2±0.113‰ VPDB. The $\delta^{13}C$ values ranged from −21.1 to −19.3‰ and the average value is −19.8‰ VPDB. Based upon the paleotemperature gradient of Spicer and Corfield (1992), the estimated soil groundwater $\delta^{18}O$ values for the Lower Tuscaloosa Formation ranged from −7.0 to −6.1‰ VSMOW (Fig. 5).

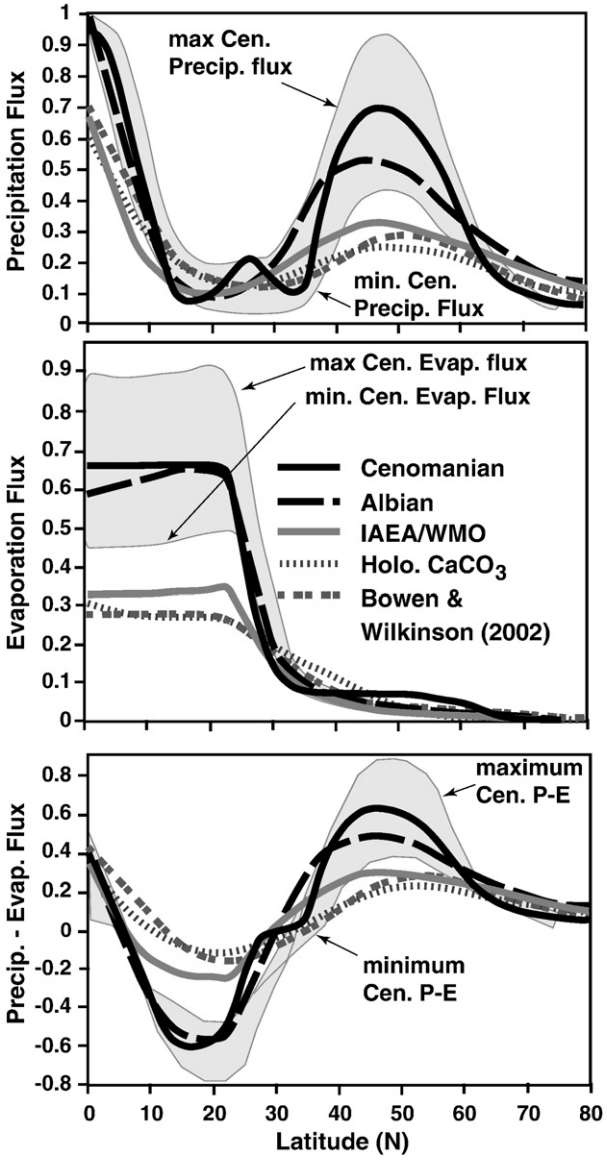

Fig. 6. The graphs illustrate the precipitation (A), evaporation (B), and precipitation–evaporation (C) latitudinal profiles used in the mass-balance modeling experiments. The precipitation and evaporation fluxes are dimensionless quantities of vapor added (precipitation) or removed (evaporation) from the theoretical airmasses as they progress from the equator toward the North Pole via Hadley, Ferrell, and Polar cell circulation. The mass-balance model recomputed the isotopic values of the air mass vapor with each step in latitude based upon the temperature, relative humidity, feedback moisture $\delta^{18}O$ values, precipitation flux, evaporation flux, and the vapor $\delta^{18}O$ value from the previous step. The light gray shading illustrates the range of values (error) that may be input into the model to reproduce the Cenomanian latitudinal gradient in siderite $\delta^{18}O$ values.

3.2.2. Dakota Formation RCP

The $\delta^{18}O$ and $\delta^{13}C$ values of the sphaerosiderites from the 8.6 m interval of the RCP section define a meteoric sphaerosiderite line (Ludvigson et al., 1998) with an average $\delta^{18}O$ value of −5.05±0.27‰ VPDB. The 7.6 m interval defines a meteoric sphaerosiderite line with an average value of −4.1±0.124‰ VPDB. The $\delta^{18}O$ values range from −5.5‰ to −4.7‰ VPDB and the $\delta^{13}C$ values range from −19.1‰ to −14.1‰VPDB for the 8.6 m interval. The $\delta^{18}O$ values range from −4.4‰ to −4.0‰ VPDB and the $\delta^{13}C$ values range from −11.9‰ to −6.7‰VPDB for the 7.6 m interval. The MSL values are a proxy for estimated meteoric water $\delta^{18}O$ values ranging from −7.0‰ to −5.0‰ VSMOW.

3.2.3. Dunvegan Formation

The Kaskatinaw Gorge sphaerosiderites yield $\delta^{18}O$ compositions that define an MSL of −12.5±0.312‰ VPDB. The $\delta^{18}O$ values range from −13.1 to −12.1‰ VPDB and the $\delta^{13}C$ values range from −10.1 to −8.9‰ VPDB. Based upon the paleotemperature gradient of Spicer and Corfield (1992), the estimated soil groundwater $\delta^{18}O$ values for the Dunvegan Formation ranged from −16.0 to −15.7‰ VSMOW.

3.3. Mass-balance modeling results

The three different modern/Holocene gradients that were used to calibrate the mass-balance model generated very similar results. The precipitation and evaporation flux profiles with latitude vary by a maximum of 0.16 at any given latitude. The temperature gradients, continental vapor feedback $\delta^{18}O$ values, relative humidity, and $\delta^{18}O$ of ocean water input values (or trends) were all held constant for these simulations. Each of the modern simulations showed a peak in precipitation flux in the tropics, decreased values in the 10–30° latitudinal range, a secondary peak in precipitation fluxes between 45 and 55°N, and values tapering off toward the pole (Fig. 6). There is a maximum difference between the precipitation flux values of 28% at 5°, 50% at 25°, 30% at 45°, and 100% at 75°N latitude for the modern model simulations.

The Cenomanian was modeled to reproduce the sphaerosiderite $\delta^{18}O$ gradient that ranges from −4.0 to −12.5‰ VPDB over the range of 25–55°N paleolatitudes. The maximum range of error in the $\delta^{18}O$ data from each location were used to estimate the upper and lower limits of the precipitation and evaporation fluxes (Fig. 7). The minimum values include a gradient that ranged from −4 to −9.0‰ VPDB over the range 25–65° N latitude. This simulation uses the calculated equivalent siderite $\delta^{18}O$ values for the Dunvegan Formation based upon the groundwater $\delta^{18}O$ values of Vitali et al. (2002) estimated from clay mineral stable isotopic analyses (discussed below). The higher paleolatitude was used to estimate the potential error in the model related to varying paleogeographic reconstructions (e.g. Irving et al., 1993; Witzke, 2003). The gray shaded areas on Figs. 6–9 reflect the estimated range in error of the model estimates propagated from the maximum range in $\delta^{18}O$ values and the potential variance in the paleolatitudinal reconstructions.

By comparison, the Cenomanian precipitation flux profiles are significantly different from the three modern precipitation flux profiles. The most noteworthy differences are between 10–20°, 20–30°, and 35–55°N latitudes (Fig. 6). A 1.6 to 1.8× increase in precipitation flux was modeled at 25°N, and a 2.2 to 2.5× increase in precipitation flux is modeled at 45°N for the Cenomanian. A 2.3 to 2.5×

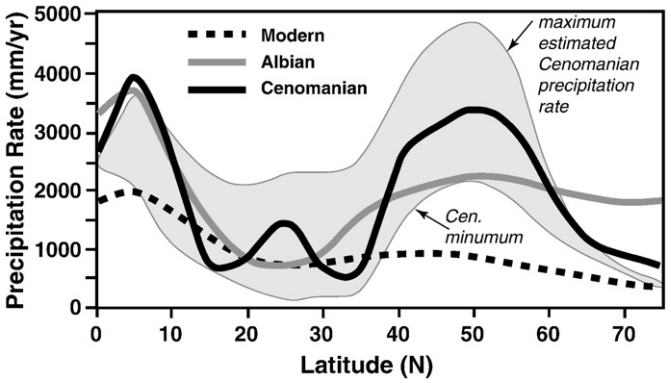

Fig. 8. The graph illustrates estimated precipitation rates for the KWIB during the Albian and Cenomanian with modern precipitation rates for comparison. The Cenomanian estimates range between two different modeling scenarios (High and Low) with the "High" estimates based upon the steep paleolatitudinal trend with the sphaerosiderite proxy data from the Dunvegan Formation (average: −12.5‰ VPDB). The "Cenomanian Low" estimates use the siderite-equivalent $\delta^{18}O$ value of (−8.0 to −9.5‰ VPDB) for the Dunvegan Formation based upon the meteoric $\delta^{18}O$ values of Vitali et al. (2002). The shaded area between 35 and 55°N above the Cenomanian Low curve represents the estimated range of precipitation rates based upon the range in $\delta^{18}O$ values from Vitali et al. (2002).

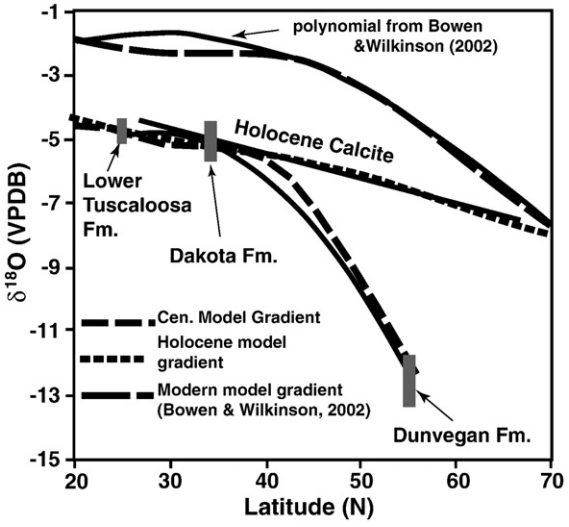

Fig. 7. The graph illustrates the polynomial trends that are fit to the empirical (and theoretical) modern and Cretaceous data, and the mass-balance model generated gradients (dashed lines). The mass-balance model is designed to reproduce the latitudinal trend in empirical siderite (or calcite) $\delta^{18}O$ values.

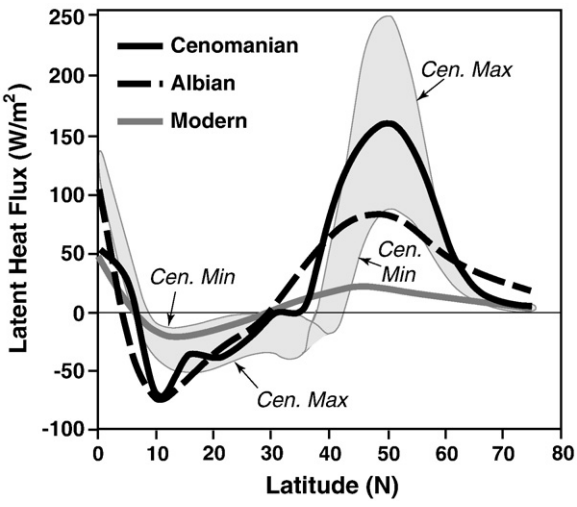

Fig. 9. The curves denote latitudinal domains of heat gain (positive values) vs. heat loss (negative values) over the North American continent for the present, Albian, and Cenomanian time. The values represent long-term estimates of the average heat (W/m^2) lost from the tropics to evaporating water vapor, and heat released (gained) in the mid–high latitudes through the condensation of water vapor.

decrease in precipitation flux compared to the modern simulations is modeled for 15°N paleolatitude. Between 55 and 80°N latitudes, the Cenomanian precipitation flux profile is very similar to the modern precipitation flux values.

The evaporation flux profiles for the Cenomanian are significantly elevated in the low latitudes compared to all of the modern model simulations (Fig. 6). The Cenomanian was modeled with evaporation fluxes that are approximately 2.4× greater at 5°N latitude and 1.8× greater than the modern at 25°N latitude.

3.4. Precipitation rate estimates

Using the precipitation flux values calculated from the model coupled with the paleotemperature estimates (Wolfe and Upchurch, 1987; Spicer and Corfield, 1992), modern mean annual temperatures, and modern, zonally-averaged mean annual precipitation rates, estimates of paleoprecipitation rates can be calculated for the KWIB (Ufnar et al., 2002, 2004b). The saturation vapor pressure of the Cenomanian atmosphere would have been significantly greater than that of the present particularly in the higher latitudes. The modeled precipitation flux values are an estimate of the long-term average fraction of vapor removed from airmasses at a given latitude. Using the modern zonally averaged rainfall rate for a given latitude (e.g. mid-continent, North America, 45°N, approximately 1000 mm/yr; Aguado and Burt, 2004), and the modern modeled precipitation flux values, we can estimate the potential precipitation rate. The potential precipitation rate (PPR) represents the amount of rainfall that would occur on average if the atmosphere were to completely exhaust its moisture supply. This is unrealistic however; it provides a value by which we can compare the saturation vapor pressures of the modern to the ancient. Using the equation $(0.0002T^3+0.0111T^2+0.321T+4.8$; Clark and Fritz, 1997), the saturation vapor pressure at 45°N has an average value of 10.3 g/m^3 based upon a mean annual temperature of 11.5 °C. With an estimated mid-Cretaceous MAT of 19.1 °C (Wolfe and Upchurch, 1987; Spicer and Corfield, 1992) at 45°N, the average saturation vapor pressure would have been 16.3 g/m^3, approximately 59% greater than present. The precipitation flux for the modern simulations ranges from 0.26 to 0.34. Using equation 4 of Ufnar et al. (2002), the modern zonally-averaged precipitation rate at 45°N (1000 mm/yr) divided by the modeled precipitation flux values (0.28–0.32), results in a PPR ranging from 3100 to 3600 mm/yr. If the Cenomanian atmosphere could hold 59% more water vapor, then the equivalent PPR would have ranged from 4900 to 5700 mm/yr. The modeled Cenomanian fluxes for 45°N range from 0.42 to 0.93 with the best scenario value of 0.73, thus multiplying the precipitation fluxes by the PPR values results in precipitation rate estimates ranging from 2000 to 5200 mm/yr, with a best scenario value of 3600 mm/yr. The equator-pole precipitation rate estimates through the KWIB are significantly greater in the tropics and the mid-latitudes compared to modern precipitation rates (Fig. 8). The precipitation rates estimated for the Cenomanian are also potentially greater than those estimated for the Albian in the mid-latitudes (Ufnar et al., 2002).

3.5. Latent heat flux calculations

The modeled precipitation and evaporation fluxes and estimated precipitation rates were used to estimate changes in latent heat flux over the KWIB during the Cenomanian Stage (Fig. 9). The methods of Ufnar et al. (2004c) were used to calculate long-term average latent heat flux (LHF) values in W/m^2. The theoretical estimates are for one square meter of ground surface along a North–South latitudinal transect through the KWIB. The temperature-dependent equation for the latent heat of vaporization, $Q=Lm$ (Q=heat in calories, m=mass of H_2O in kilograms, and L is a temperature-dependent variable), was used to calculate heat loss or gain along the latitudinal transect. The term L varies as a linear function between 0 and 100 °C [$-0.57(T)+597$ cal/g; T = temperature in °C] (Ufnar et al., 2004a,b,c). Fig. 6 illustrates the modeled difference in moisture balance between the modern and Cenomanian. The moisture deficit in the low latitudes (10–20°N) based upon the modeled precipitation minus evaporation flux values (P–E) is approximately 5.5× greater in the Cenomanian simulations compared to the modern. The moisture surplus (40–60°N) based upon the P–E values is approximately 2.3× greater than the modern values in the Cenomanian simulation.

The present moisture deficit in the tropics is on the order of −8.6 W/m^2 at 20°N latitude (the negative value indicates a net heat loss). The estimated LHF values for the Cenomanian are approximately 3.4× greater at 20°N (3.0 to 3.4× greater than present). The moisture surplus at 50°N latitude presently equates to a heat gain of 17 W/m^2. The peak at 50°N in the Cenomanian simulation equates to an LHF value of 180 W/m^2. The LHF in the mid latitudes during the Cenomanian is estimated to have been 10.6× greater than the present.

4. Discussion

The modeling results for the Cenomanian Stage in the KWIB are somewhat different from those of the Albian (Fig. 6; Ufnar et al., 2002, 2004c). The “bump” in the Cenomanian precipitation flux profile around 25°N was necessitated to generate δ^{18}O values that are only slightly depleted relative to the δ^{18}O values at 35°N paleolatitude. The Albian model results suggest that 25°N was an area of significant moisture deficit. The Cenomanian model results and the lithofacies suggest that during the Cenomanian, the eastern margin of the Western Interior Seaway at approximately 25°N paleolatitude was not excessively dry. The sphaerosiderites of the Lower Tuscaloosa fall within a domain that the Cenomanian model results suggest was an area of near moisture balance with P–E values ranging from −0.2 to 0.06. The moisture balance is supported by GENESIS model results of the early Turonian that illustrate the 0 mm/day contour for P–E in the geographic area occupied by the sampled intervals of the Lower Tuscaloosa (Slingerland et al., 1996). The LHF values range from a slight heat deficit of −22 W/m^2 at 25°N to a moisture balance of 0 W/m^2 at 30°N. The precipitation rate estimates from this study are on the order of 1500–1800 mm/yr. Current mean annual precipitation rates at 25°N in North America (e.g. near Brownsville, Texas) are on the order of 635 mm/yr; however the potential evapotranspiration rates are more than 2× that (1400 mm/yr; Fipps et al., 2006). The precipitation rates at 25°N during the Cenomanian were more like they are in coastal Mississippi at present, ranging from 1400–1600 mm/yr (NOAA Climatic Data Center, 2008). Several thin (30–50 cm), coal seams and highly carbonaceous mudstone intervals are observed in the Lower Tuscaloosa Formation (Mancini et al., 1987; Cameron et al., 1992). Also, the pedogenically modified interfluvial deposits are characterized by an abundance of clay coatings, pedogenic slickensides, and striated b-fabrics all suggesting well-drained conditions, with frequent wetting and drying cycles (FitzPatrick, 1984; McCarthy et al., 1998, 1999a).

There are no indicators for a significant moisture deficit nor arid paleoclimatic conditions in the Lower Tuscaloosa Formation of southwestern Mississippi. Conversely, paleosols developed in the Lower Albian upper Glen Rose Formation near Austin, Texas (25°N paleolatitude) are characterized by pedogenic calcretes and positive covariant trends in δ^{18}O vs. δ^{13}C values suggesting substantial evaporative enrichment of vadose fluids (Ludvigson et al., 2005; Ufnar et al., 2005a,b). A meteoric calcite line (MCL: −3.8‰ VPDB) defined for the Upper Glen Rose Formation yields estimated meteoric δ^{18}O values ranging from −2.0 to −1.6‰ VSMOW. These estimates are significantly enriched relative to those estimated for the Lower Tuscaloosa (−6.8 to −4.5‰ VSMOW) from the same paleolatitude. The vast difference in the soils and meteoric water values may be related to changes in sea-level and paleoceanographic circulation between the Early Albian and the Cenomanian.

The Late Albian was characterized by lower eustatic sea-level compared to the Cenomanian (Haq et al., 1987), and the Late Albian of the KWIB is marked by a significant regression and coastal offlap (Kauffman and Caldwell, 1993). The Glen Rose paleosol described above is a sequence-bounding paleosol that marks the unconformity surface between the Edwards Group and the overlying Fredricksburg Group (Moore, 1996; Talbert and Atchley, 2000; Mancini and Puckett, 2005). The Upper Glen Rose paleosol developed during the regressive phase of sea-level prior to the T5 maximum transgression of the Kiowa–Skull Creek cycle in the KWIB (Kauffman, 1969, 1977; Caldwell, 1984; Kauffman and Caldwell, 1993; Talbert and Atchley, 2000). The Kiowa–Skull Creek cycle was one of the first times in which the northern and southern arms of the western interior seaway were able to flood across the continental arch, connect and mix (Kauffman, 1969, 1977; Caldwell, 1984; Stelck and Koke, 1987; Kauffman and Caldwell, 1993). However, the paleosol developed in the Upper Glen Rose likely developed during a regressive phase preceding this cycle (Fig. 10), as the southern arm of the seaway was retreating and was isolated from the northern, cooler water connection.

The paleosols of the Lower Tuscaloosa most-likely developed during the multiple sea-level fluctuations that occurred during the initial Cenomanian transgression of the Greenhorn Cycle in the KWIB (Fig. 10; Kauffman and Caldwell, 1993). The Western Interior Seaway was fully connected between the proto-Gulf of Mexico and the Boreal Sea during that time, and peak flooding during the latest Cenomanian may have reached elevations of 295–300 m above present sea-level (McDonough and Cross, 1991; Kauffman and Caldwell, 1993). The mixing of cool, slightly brackish northern waters with warm, subtropical normal-salinity water masses would have had a significantly different impact on precipitation patterns and rates vs. that of a retreating, isolated, warm southern arm of the seaway (Kauffman and Caldwell, 1993; Slingerland et al., 1996).

GENESIS model results for the mid-Cretaceous (early Turonian) suggest that the climate was warm, humid and non-seasonal with precipitation rates on the order of 1100 mm/yr along the northern margin of Tethys (Slingerland et al., 1996). These values are consistent with the precipitation estimates presented here as well as paleobotanical evidence from Wolfe and Upchurch (1987). Albian Community Climate Model simulations (~100 Ma) however, that do not have a fully-connected western interior seaway, predict zonally averaged precipitation rates on the order of approximately 730 mm/yr with a *P–E* value of −1.4 mm/day at 25°N paleolatitude (Barron et al., 1989). The mid-Cretaceous GENESIS model experiments of Bice and Norris (2002) that used the plate reconstruction of Barron (1987), which does not have a fully-connected KWIS, predict *P–E* values of −0.7 to −0.9 mm/day at 25°N paleolatitude. Thus, the Late Albian Commanche Shelf area (Rose, 1972; Bay, 1982) at 25°N was characterized by more arid conditions. The southeastern margin of the western interior seaway (25°N paleolatitude) was characterized by more humid and balanced *P–E* conditions during Cenomanian through early Turonian time. Thus, the mass-balance modeled difference in Albian vs. Cenomanian *P–E* flux values and precipitation rates are supported by late–Early Albian $\delta^{18}O$ values and pedogenic features of the Upper Glen Rose Formation, and CCM and GENESIS model results for the Albian and Cenomanian–Turonian respectively (Barron et al., 1989; Slingerland et al., 1996).

Both the Albian and Cenomanian mass-balance model results suggest increased precipitation rates in the mid to high latitudes compared to the present. The estimates based upon the Cenomanian mass-balance model results suggest that the precipitation rates between 40 and 50°N latitude increased significantly (approximately 40%) when compared to the estimates for the Albian (Fig. 8). An increase in mid-latitude (40–45°N) precipitation rates from the Albian to Turonian is also predicted by GENESIS modeling experiments, with an increase on the order of 15% (Poulsen et al., 1999).

Are the mass-balance model estimates excessive? It has been suggested that the sphaerosiderites from the Kaskatinaw Gorge (55°N paleolatitude) locality have been subjected to later diagenetic alterations and may not be a good proxy for precipitation $\delta^{18}O$ values (Vitali et al., 2002). Petrographic, cathodoluminescence, and microprobe analyses of the Dunvegan sphaerosiderites show no evidence for textural or geochemical alterations of the nodules. Vitali et al. (2002) present $\delta^{18}O$ water value estimates for the Dunvegan Formation that were obtained from the stable isotopic values of pedogenic clay minerals. The clay minerals yield estimated $\delta^{18}O$ values of −12.9 to −11.6‰ VSMOW for the soil groundwater (Vitali et al., 2002). These values were used to estimate equivalent siderite values of −8 to −9.5‰ VPDB for the Cenomanian minimum simulations using the paleotemperature estimates of Wolfe and Upchurch (1987). The $\delta^{18}O$ values of the pedogenic clays should reflect that of the water involved in the weathering reactions (Faure, 1986). Thus, the pedogenic clay $\delta^{18}O$ values provide a reasonable alternative proxy, however the clays formed under significantly different conditions than the sphaerosiderites. The equivalent siderite values determined from the $\delta^{18}O$ values of Vitali et al. (2002) are close to the siderite values obtained from the Late Albian Boulder Creek and Peace River Formations (52°N paleolatitude) of western Canada (−11 to −8.5‰; Ufnar et al., 2001, 2005a,b,c). The Cenomanian minimum simulations yield more conservative precipitation flux values and precipitation rate estimates. Precipitation rates at 45°N are estimated to be approximately 2300 mm/yr using the $\delta^{18}O$ values of Vitali et al. (2002) compared to 2100 mm/yr for the Albian model (Ufnar et al., 2002). This results in a 9% increase in Cenomanian precipitation rates relative to the Albian and is consistent with the GENESIS results of Poulsen et al. (1999). The Cenomanian minimum precipitation rate estimates are also much closer to the Late Cenomanian–Early Turonion GENESIS precipitation rates estimated for 25–41°N in North America by Flöegel et al. (2005) which are on the order of 1600 mm/yr (Cenomanian minimum estimates at 41°N are 1500 mm/yr). The Cenomanian best scenario values obtained from this investigation are probably more

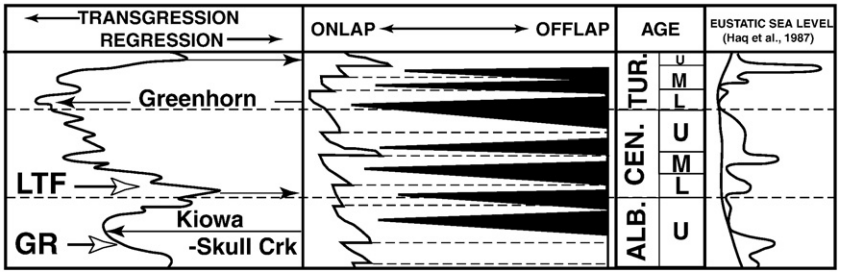

Fig. 10. The chart illustrates transgressive–regressive cycles, onlap–offlap cycles, and eustatic sea-level changes during the mid-Cretaceous (modified from Kauffman and Caldwell, 1993). The approximate position of the upper Glen Rose Formation (GR) paleosol described in the text is shown by the white arrow on the left (age determined from Talbert and Atchley, 2000). The approximate position of the beginning of Lower Tuscaloosa Formation deposition is also illustrated (LTF, white arrow) during the early transgressive phase of the Greenhorn Cycle.

representative of the North American western interior precipitation rates, and the Cenomanian minimum estimates are more conservative, and may be more representative of average Northern Hemisphere values during the Cenomanian. In either scenario, the Cenomanian mid-latitude precipitation rates (40–50°N) are significantly higher than those of the present, and based upon the sphaerosiderite values there is a marked increase from those of the Albian.

The Cenomanian simulation has identical evaporation flux values to the Albian from 0 to 20°N paleolatitude, however the values drop off more rapidly between 22 and 38°N. Between 40 and 60°N the evaporation fluxes for the Cenomanian simulations were significantly greater than those of the Albian. The Cenomanian minimum simulation had significantly lower evaporation fluxes in the low latitudes (0–20°N), similar values between 22 and 35°N, and identical values to the Albian for latitudes greater than 35°N. The depleted $\delta^{18}O$ values of the lower Tuscaloosa Formation necessitated a greater balance between precipitation and evaporation flux between 20 and 35°N in the Cenomanian best scenario simulation. However, increased vapor feedback was needed in the higher latitudes to generate $\delta^{18}O$ values similar to the Dunvegan Formation sphaerosiderites. Decreased evaporation flux values in the tropics were needed to produce a shallower $\delta^{18}O$ gradient in the mid to high latitudes for the Cenomanian minimum simulation.

The implications for net transfer of heat through the atmosphere are significantly different in the Cenomanian modeling experiments compared to earlier investigations of the Albian (Ufnar et al., 2004a,b,c). The Cenomanian simulations suggest a massive increase in heat transfer to the atmosphere between 40 and 50°N paleolatitude. The LHF values calculated from the Albian model simulations are estimated to have been 3.6× present values at 45°N (Ufnar et al., 2004a,b,c), The estimates based upon the Cenomanian high experiments presented here suggest LHF values were approximately 10.6× the present at 45°N. More conservative estimates based upon the Cenomanian Low experiments suggest a 4.2× increase in LHF compared to the modern. In the Cenomanian experiments, the total heat exported from the tropical dry-belt is reduced relative to the Albian, and LHF to the higher latitudes, north of 55° is reduced relative to the Albian. The lithofacies and $\delta^{18}O$ values of the lower Tuscaloosa Formation suggest that conditions in the southeastern portion of the KWIB were much less arid during the early Cenomanian than they were during the early Albian. Thus, the LHF estimates for the tropical dry-belt are reduced in the Cenomanian relative to the Albian, however they are still greater than that of the present. High-latitude sphaerosiderite data are needed to better constrain the heat flux estimates for the high latitudes during the Cenomanian. The large increase in LHF predicted for 45°N may be reduced to values more comparable with those estimated for the Albian, and the higher latitudes might be characterized by increased LHF values.

The empirical latitudinal trend in meteoric sphaerosiderite $\delta^{18}O$ values for the Cenomanian of the KWIB reinforces the concept of an intensified hydrologic cycle during greenhouse-world time periods. These data demonstrate that North American mid-latitude precipitation rates were much higher than present, and perhaps greater than they were during the Albian. Transfer of heat through the atmosphere was also an important process during the Cenomanian, however the distribution of that heat may have been quite different from the Albian. The empirical and modeled paleoclimatological differences between the Albian and Cenomanian are interpreted to be closely linked to paleoceanographic variations associated with sea-level changes between the Kiowa–Skull Creek and Greenhorn cyclothems in the KWIB (Kauffman and Caldwell, 1993). The variability in the Albian vs. Cenomanian sphaerosiderite $\delta^{18}O$ paleolatitudinal trends and modeling results underscores the need to reconstruct paleoclimatological conditions from multiple time-slices during the mid-Cretaceous in an effort to better understand the dynamics of a greenhouse world hydrologic cycle.

5. Conclusions

(1) The empirical paleolatitudinal trend in sphaerosiderite $\delta^{18}O$ values form the Cenomanian of the KWIB is steeper and more depleted than that of the modern and the Albian reconstruction of Ludvigson et al. (1998) and Ufnar et al. (2002).

(2) Stable isotope mass-balance modeling results suggest that Cenomanian tropical precipitation rates were approximately 1.8× present values (5°N), mid-latitude precipitation rates were approximately 3.6× present values (45–50°N), and high-latitude precipitation rates were approximately 2.0× present values (75°N). The subtropical dry belt precipitation rates were approximately 2.5× less than modern rates at 15°N and 1.9× greater at 25°N.

(3) The increased evaporation/evapotranspiration and precipitation rates in the Cenomanian contributed significantly to the transfer of heat through the atmosphere as Latent Heat. The average heat export from the subtropics via evaporation was approximately 3.4× present values (−29 W/m^2, Cenomanian vs. −8.6 W/m^2, present) and the average amount of heat released due to condensation in the mid-latitudes was up to 10.6× present values (180 W/m^2, Cenomanian vs. 17 W/m^2, present).

(4) The intensified hydrologic cycle of the mid-Cretaceous may have contributed to the reduced equator-to-pole temperature gradients and a more equable global climate. The high sea-level and extensive continental flooding that occurred during the Greenhorn Cyclothem (Kauffman and Caldwell, 1993) may have resulted in the steeper paleolatitudinal trend in meteoric $\delta^{18}O$ values compared to those of the Albian Stage (Ufnar et al., 2002).

References

Aguado, E., Burt, J.E., 2004. Understanding Weather and Climate, Third edition. Pearson Education, Inc., Upper saddle River, NJ. 560 pp.

Baker, A., Ito, E., Smart, P.L., McEwan, R.F., 1997. Elevated and variable values of ^{13}C in speleothems in a British cave system. Chem. Geol. 136, 263–270.

Bar-Matthews, M., Ayalon, A., Gilmour, M., Matthews, A., Hawkesworth, C.J., 2003. Sea-land oxygen isotopic relationships from planktonic foraminifera and speleothems in the Eastern Mediterranean region and their implication for paleorainfall during interglacial intervals. Geochim. Cosmochim. Acta 67, 3181–3199.

Barron, E.J., 1987. Cretaceous plate tectonic reconstructions. Palaeogeogr. Palaeoclimatol. Palaeoecol. 59, 3–29.

Barron, E.J., Hay, W.W., Thompson, S., 1989. The hydrologic cycle: a major variable during Earth history. Palaeogeogr. Palaeoclimatol. Palaeoecol. 75, 157–174.

Barron, E.J., Fawcett, P.J., Peterson, W.H., Pollard, D., Thompson, S.L., 1995. A "simulation" of mid-Cretaceous climate. Paleoceanography 10, 953–962.

Bay, A.R., 1982. Evolution and porosity of carbonate shoaling cycles Lower Cretaceous–Lower Glen Rose, south Texas. Trans. — Gulf Coast Assoc. Geol. Soc. 32, 101–119.

Bice, K.L., Norris, R.D., 2002. Possible atmospheric CO_2 extremes of the Middle Cretaceous (late Albian–Turonian). Paleoceanography 17, 1070–1087.

Bowen, G.J., Wilkinson, B., 2002. Spatial distribution of $\delta^{18}O$ in meteoric precipitation. Geology 30, 315–318.

Brewer, R., 1964. Fabric and Mineral Analysis of Soils. John Wiley & Sons, New York. 470 pp.

Bullock, P., Fedoroff, N., Jongerius, A., Stoops, G., Tursina, T., Babel, U., 1985. Handbook for Soil Thin Section Description. Waine Res. Pubs., Wolverhampton. 152 pp.

Caldwell, W.G.E., 1984. Early Cretaceous transgressions and regressions in the southern interior plains. In: Stott, D.F., Glass, D.J. (Eds.), The Mesozoic of Middle North America. Can. Soc. Petrol. Geol. Mem., vol. 9, pp. 173–203.

Cameron, C.P., Patrick, D.M., Keith, C.D., 1992. Authigenic clay mineral distribution, Lower Tuscaloosa Formation, southwest Mississippi: impact on sandstone reservoir quality in the North Hustler Field area. Trans. — Gulf Coast Assoc. Geol. Soc. 52, 47–59.

Carothers, W.W., Lanford, H.A., Rosenbauer, R.J., 1988. Experimental oxygen isotope fractionation between siderite–water and phosphoric acid liberated CO_2–siderite. Geochim. Cosmochim. Acta 52, 2445–2450.

Clark, I., Fritz, P., 1997. Environmental Isotopes in Hydrogeology. Lewis Publishers, Boca Raton, FL.

Covey, C., Barron, E.J., 1988. The role of ocean heat transport in climate change. Earth-Sci. Rev. 24, 429–445.

Crowley, T.J., 1991. Past CO_2 changes and tropical sea surface temperatures. Paleoceanography 6, 387–394.

Dansgaard, W., 1964. Stable isotopes in precipitation. Tellus 16, 436–468.

DeConto, R.M., Hay, W.W., Thompson, S.L., Bergengren, J., 1999. Late Cretaceous climate and vegetation interactions: cold continental interior paradox. In: Barrera, E., Johnson, C.C. (Eds.), Evolution of the Cretaceous Ocean–Climate System. Geol. Soc. of Amer. Sp. Pap., vol. 332, pp. 391–406.

Denniston, R.F., Gonzalez, L.A., Asmerom, Y., Baker, R.G., Reagan, M.K., Bettis III, E.A., 1999a. Evidence for increased cool season moisture during the middle Holocene. Geology 27, 815–818.
Denniston, R.F., Gonzalez, L.A., Backer, R.G., Asmerom, Y., Reagan, M.K., Edwards, R.L., Alexander, E.C., 1999b. Speleothem evidence for Holocene fluctuation of the prairie-forest ecotone, north-central USA. The Holocene 9, 671–676.
Dettman, D.L., Lohman, K.C., 2000. Oxygen isotope evidence for high-altitude snow in Laramide Rocky Mountains of North America during the Late Cretaceous and Paleogene. Geology 28, 243–246.
Faure, G., 1986. Principles of Isotope Geology, second edition. John Wiley and Sons, New York. 589 pp.
Fipps, G., Jones, A., Braden, C., 2006. Irrigation technology center. http://itc.tamu.edu/ website of the Irrigation Technology Center, a center of the Texas Water Resources Institute. Texas A&M University.
FitzPatrick, E.A., 1984. Micromorphology of Soils. Chapman & Hall, New York. 433 pp.
Flöegel, S., Hay, W.W., DeConto, R.M., Balukhovsky, A., 2005. Formation of sedimentary bedding couplets in the Western Interior Seaway of North America — implications from Climate System Modeling. Palaeogeogr. Palaeoclimatol. Palaeoecol. 218, 125–143.
Frumkin, A., Carmi, I., Gopher, A., Ford, D.C., Schwarcz, H.P., Tsuk, T., 1999. A Holocene millennial-scale climatic cycle from a speleothem in Nahal Qanah Cave, Israel. The Holocene 9, 677–682.
Gonfiantini, R., 1986. Environmental isotopes in lake studies. In: Fritz, P., Fontes, J.Ch. (Eds.), Handbook of Environmental Isotope Geochemistry. The Terrestrial Environment, B., vol. 2. Elsevier, Amsterdam, The Netherlands, pp. 113–168.
Gröcke, D.R., Ludvigson, G.A., Witzke, B.L., Robinson, S.A., Joeckel, R.M., Ravn, R.L., Ufnar, D.F., 2006. Recognition of the Albian–Cenomanian (OAE1d) sequence boundary using terrestrial-plant carbon isotopes: Dakota Formation, in the Western Interior Basin, USA. Geology 34, 193–196.
Haq, B.V., Hardenbol, J., Vail, P.R., 1987. Chronology of the fluctuating sea levels since the Triassic. Science 235, 1159–1167.
Hay, W.W., DeConto, R.M., 1999. Comparison of modern and Late Cretaceous meridional energy transport and oceanology. In: Barrera, E., Johnson, C.C. (Eds.), Evolution of the Cretaceous Ocean–Climate System. Geol. Soc. of Amer. Sp. Pap., vol. 332, pp. 73–90.
Horvantinčič, N., Bronic, I.K., Obelic, B., 2003. Differences in the ^{14}C age, $\delta^{14}C$ and $\delta^{18}O$ of Holocene tufa and speleothem in the Dinaric Karst. Palaeogeogr. Palaeoclimatol. Palaeoecol. 193, 139–157.
Huber, B.T., Hodell, D.A., Hamilton, C.P., 1995. Mid- to Late Cretaceous climate of the southern high latitudes: stable isotopic evidence for minimal equator-to-pole thermal gradients. Geol. Soc. Amer. Bull. 107, 1164–1191.
Irving, E., Wynne, P.J., Bloberman, B.R., 1993. Cretaceous paleolatitudes and overprints of North American Craton. In: Caldwell, W.G.E., Kauffman, E.G. (Eds.), Evolution of the Western Interior Basin. Sp. Pap. — Geol. Assoc. Can., vol. 39, pp. 91–96.
Kauffman, E.G., 1969. Cretaceous marine cycles of the Western Interior. Mt. Geol. 6, 227–245.
Kauffman, E.G., 1977. Geological and biological overview: Western Interior Cretaceous Basin. In: Kauffman, E.G. (Ed.), Cretaceous Facies, Faunas, and Paleoenvironments Across the Western Interior Basin: Field Guide, North American Paleontological Convention II. Mount. Geol., vol. 14, pp. 75–99.
Kauffman, E.G., Caldwell, W.G.E., 1993. The Western Interior Basin in space and time. In: Caldwell, W.E.G., Kauffman, E.G. (Eds.), Evolution of the Western Interior Basin. Geol. Assoc. Can. Sp. Pap., vol. 39, pp. 1–30.
Kraus, M.J., Hasiotis, S.T., 2006. Significance of different modes of rizolith preservation to interpreting paleoenvironmental and paleohydrologic settings: examples from paleogene paleosols, Bighorn Basin,Wyoming, U.S.A. J. Sediment. Res. 76, 633–646.
Larson, R.L., 1991. Geological consequences of superplumes. Geology 19, 963–966.
Linge, H., Lauritzen, S.-E., Lundberg, J., Berstad, I.M., 2001. Stable isotope stratigraphy of Holocene speleothems; examples from a cave system in Rana, Northern Norway. Palaeogeogr. Palaeoclimatol. Palaeoecol. 167, 209–224.
Lohmann, K.C., 1988. Geochemical patterns of meteoric diagenetic systems and their application to studies of paleokarst. In: James, N.P., Choquette, P.W. (Eds.), Paleokarst. Springer Verlag, Berlin, pp. 58–80.
Ludvigson, G.A., González, L.A., Metzger, R.A., Witzke, B.J., Brenner, R.L., Murillo, A.P., White, T.S., 1998. Meteoric sphaerosiderite lines and their use for paleohydrology and paleoclimatology. Geology 26, 1039–1042.
Ludvigson, G.A., Ufnar, D.F., Gonzalez, L.A., Witzke, B.J., Brenner, R.L., 2005. Reconciling the stable isotopic paleohydrology of pedogenic siderites and calcites, North-Central Section — 39th Annual Meeting (May 19–20, 2005). Geol. Soc. Amer. Abstr. Prog. 37, 86.
Majoube, M., 1971. Fractionnement en oxygène-18 et en deutérium entre l'eau et as vapeur. J. Chem. Phys. 197, 1423–1436.
Mancini, E.A., Puckett, 2005. Jurassic and Cretaceous transgressive–regressive (T–R) cycles, northern Gulf of Mexico, USA. Stratigraphy 2, 31–48.
Mancini, E.A., Mink, R.M., Payton, J.W., Beardon, B.L., 1987. Environments of deposition and petroleum geology of Tuscaloosa Group (Upper Cretaceous), South Carlton and Pollard Fields, southwestern Alabama. Am. Assoc. Pet. Geol. Bull. 71, 1128–1142.
McCarthy, P.J., Plint, A.G., 1999. Floodplain paleosols of the Cenomanian Dunvegan Formation, Alberta and British Columbia, Canada: Micromorphology, pedogenic processes, and paleoenvironmental implications. In: Marriott, S.B., Alexander, J. (Eds.), Floodplains: Interdisciplinary Approaches. Geol. Soc. Amer. Sp. Pap., vol. 163, pp. 289–310.
McCarthy, P.J., Martini, I.P., Leckie, D.A., 1998. Pedogenic and diagenetic influences on void coating formation in Lower Cretaceous paleosols of the Mill Creek Formation, southwestern Alberta, Canada. Geoderma 87, 209–237.
McCarthy, P.J., Martini, I.P., Leckie, D.A., 1999a. Pedogenic and diagenetic influences on void coating formation in Lower Cretaceous paleosols of the Mill Creek Formation, southwestern Alberta, Canada. Geoderma 87, 209–237.
McCarthy, P.J., Faccini, U., Plint, A.G., 1999b. Evolution of an ancient coastal plain: paleosols, interfluves and alluvial architecture in a sequence stratigraphic framework, Cenomanian Dunvegan Formation, NE British Columbia, Canada. Sedimentology 46, 861–892.
McDonough, K.J., Cross, T., 1991. Late Cretaceous sea level from a paleoshoreline. J. Geophys. Res. 96, 6591–6607.
Moore, C.H., 1996. Anatomy of a sequence boundary — Lower Cretaceous Glen Rose/Fredricksburg, Central Texas platform. Trans. Gulf Coast Assoc.Geol. Soc. 46, 313–331.
Niggemann, S., Mangini, A., Richter, D.K., Wurth, G., 2003a. A paleoclimate record of the last 17,600 years in stalagmites from the B7 cave, Sauerland, Germany. Quat. Sci. Rev. 22, 555–567.
Niggemann, S., Mangini, A., Mudelsee, M., Richter, D.K., Wurth, G., 2003b. Sub-Milankovitch climatic cycles in Holocene stalagmites from Sauerland, Germany. Earth Planet. Sci. Lett. 216, 539–547.
NOAA Climatic Data Center, 2008. http://www.ncdc.noaa.gov/oa/ncdc.html.
Onac, B.P., Constantin, S., Lundberg, J., Lauritzen, S.-E., 2002. Isotopic climate record in a Holocene stalagmite from Ursilor Cave (Romania). J. Quat. Sci. 17, 319–327.
Parrish, J.T., Spicer, R.A., 1988a. Middle Cretaceous woods from the Nanushuk Group, central North Slope, Alaska. Paleontology 31, 19–34.
Parrish, J.T., Spicer, R.A., 1988b. Late Cretaceous vegetation of the North Slope, Alaska: a near polar temperature curve. Geology 16, 22–25.
Poulsen, C.J., Barron, E.J., Johnson, C., Fawcett, P., 1999. Links between major climatic factors and regional oceanic circulation in the mid-Cretaceous. In: Barrera, E., Johnson, C.C. (Eds.), Evolution of the Cretaceous Ocean–Climate System. Geol. Soc. of Amer. Sp. Pap., vol. 332, pp. 73–90.
Rind, D., Chandler, M., 1991. Increased ocean heat transports and warmer climate. J. Geophys. Res. 96, 7437–7461.
Rose, P.R., 1972. Edwards Group, Surface and Subsurface. Univ. of Texas Bureau of Econ. Geol. Rpt of Investig, Central Texas. 74, 198 pp.
Rozanski, K., Araguas-Araguas, L., Gonfiantini, R., 1993. Isotopic patterns in modern global precipitation. In: Swart, P.K., Lohmann, K.C., McKenzie, J., Savin, S. (Eds.), Climate Change in Continental Isotopic Records. Amer. Geophys. Un. Geophys. Mono., vol. 78, pp. 1–36.
Schmidt, G.A., Mysak, L.A., 1996. Can poleward ocean heat flux explain the warm equable Cretaceous climate? Paleoceanography 11, 579–593.
Schneider, S.H., Thompson, S.L., Barron, E.J., 1985. Mid-Cretaceous continental surface temperatures: are high CO_2 concentrations needed to simulate above-freezing winter conditions. In: Sundquist, E.T., Broeker, W.S. (Eds.), The Carbon Cycle and Atmospheric CO_2: Natural Variations, Archean to Present, Washington, DC. Amer. Geophys. Un. Geophys. Mono., vol. 32, pp. 554–560.
Shackleton, N.J., Kennett, J.P., 1975. Late Cenozoic oxygen and carbon isotopic changes at DSDP site 284: implications for glacial history of the Northern Hemisphere. In: Kennett, J.P., Houtz, R.E., et al. (Eds.), Initial Reports of the DSDP, 29. U.S. Gov. Print. Off., pp. 801–807.
Slingerland, R., Kump, L.R., Arthur, M.A., Fawcett, P.J., Sageman, B.B., Barron, E.J., 1996. Estuarine circulation in the Turonian Western Interior seaway of North America. Geol. Soc. Amer. Bull. 108, 941–952.
Sloan, L.C., Walker, J.C.G., Moore Jr., T.C., 1995. Possible role of oceanic heat transport in the early Eocene climate. Paleoceanography 10, 347–356.
Spicer, R.A., Corfield, R.M., 1992. A review of terrestrial and marine climates in the Cretaceous with implications for modeling the "Greenhouse Earth". Geol. Mag. 129, 169–180.
Stelck, C.R., Koke, K.R., 1987. Foraminiferal zonation of the Viking interval in the Hasler shale (Albian), northeastern British Columbia. Can. J. Earth Sci. 24, 2254–2278.
Talbert, S.J., Atchley, S.C., 2000. Sequence stratigraphy of the Lower Cretaceous (Albian) Fredricksburg Group, Central and North Texas. Trans. Gulf Coast Assoc. Geol. Soc. 50, 369–377.
Tarduno, J.A., Brinkman, D.B., Renne, P.R., Cottrell, R.D., Scher, H., Castillo, P., 1998. Evidence for extreme climatic warmth from Late Cretaceous Arctic vertebrates. Science 282, 2241–2244.
Treble, P.C., Chappell, J., Gagan, M.K., McKeegan, K.D., Harrison, T.M., 2005. In situ measurement of seasonal $\delta^{18}O$ variations and analysis of isotopic trends in a modern speleothem from southwest Australia. Earth Planet. Sci. Lett. 233, 17–32.
Ufnar, David F., McCarthy, Paul J., Ludvigson, Greg A., White, Tim S., Gonzalez, Luis A., Brenner, Robert L., 1999. Sphaerosiderite delta (super 18) O composition; a proxy for paleoprecipitation, Cenomanian Dunvegan Formation, Alberta and B.C., Canada. Geol. Soc. Amer. Abstr. Prog. 31, 279.
Ufnar, D.F., Gonzalez, L.A., Ludvigson, G.A., Brenner, R.L., Witzke, B.J., 2001. Stratigraphic implications of meteoric sphaerosiderite $\delta^{18}O$ compositions in paleosols of the Cretaceous (Albian) Boulder Creek Formation, NE British Columbia Foothills, Canada. J. Sediment. Res. 71, 1017–1028.
Ufnar, D.F., González, L.A., Ludvigson, G.A., Brenner, R.L., Witzke, B.J., 2002. The mid-Cretaceous water bearer: isotope mass balance quantification of the Albian hydrologic cycle. Palaeogeogr. Palaeoclimatol. Palaeoecol. 188, 51–71.
Ufnar, D.F., Ludvigson, G.A., González, L.A., Brenner, R.L., Witzke, B.J., 2004a. High latitude meteoric $\delta^{18}O$ compositions: paleosol siderite in the middle Cretaceous Nanushuk Formation, North Slope, Alaska. Geol. Soc. Amer. Bull. 116, 463–473.
Ufnar, D.F., González, L.A., Ludvigson, G.A., Brenner, R.L., Witzke, B.J., 2004b. Diagenetic overprinting of the sphaerosiderite paleoclimate proxy: are records of pedogenic groundwater $\delta^{18}O$ values preserved? Sedimentology 51, 127–144.
Ufnar, D.F., Ludvigson, G.A., Gonzalez, L.A., Brenner, R.L., Witzke, B.J., 2004c. Evidence for increased latent heat transport during the Cretaceous (Albian) greenhouse warming. Geology 32, 1049–1052.
Ufnar, D.F., Ludvigson, G.A., Gonzalez, L.A., Davis, J., 2005a. Mid-Cretaceous evaporation rates estimated from pedogenic carbonate isotopic values in the Glen Rose Formation, Texas. Geol. Soc. Amer. Abstr. Prog. 37, 357.

Ufnar, D.F., Ludvigson, G.A., Gonzalez, L.A., Davis, J.A., Atchley, S., 2005b. Modeling enhanced aridity from pedogenic carbonates in the mid-Cretaceous dry-belt: the Upper Glen Rose Formation, Texas, North-Central Section — 39th Annual Meeting (May 19–20, 2005). Geol. Soc. Amer. Abstr. Prog. 37, 86.

Ufnar, D.F., Ludvigson, G.A., Gonzalez, L.A., Brenner, R.L., Witzke, B.J., Leckie, D.A., 2005c. Ancient landscape development in the Late Albian Western Canadian Foreland Basin. J. Sediment. Res. 75, 984–996.

Upchurch Jr., G.R., Otto-Bliesner, B.L., Scotese, C.R., 1999. Terrestrial vegetation and its effects on climate during the Cretaceous. In: Barrera, E., Johnson, C.C. (Eds.), Evolution of the Cretaceous Ocean–Climate System. Geol. Soc. Amer. Sp. Pap., vol. 332, pp. 407–426.

Vitali, F., Longstaffe, F.J., McCarthy, P.J., Plint, A.G., Caldwell, W.G.E., 2002. Stable isotopic investigation of clay minerals and pedogenesis in an interfluve paleosol from the Cenomanian Dunvegan Formation, N.E. British Columbia, Canada. Chem. Geol. 192, 269–287.

Wang, X., Auler, A.S., Edwards, R.L., Cheng, H., Ito, E., Solheid, M., 2006. Interhemispheric anti-phasing of rainfall during the last glacial period. Quat. Sci. Rev. 25, 3391–3403.

White, T.S., Witzke, B.J., Ludvigson, G.A., Brenner, R.L., González, L.A., Ravn, R.L., 2000a. The paleoclimatological significance of Albian (mid-Cretaceous) sphaerosiderites from eastern Saskatchewan and western Manitoba. Summary of Investigations 2000, vol. 1, Saskatch. Geol. Sur. Misc. Rept., 2000-4.1, pp. 63–75.

White, T.S., Witzke, B.J., Ludvigson, G.A., 2000b. Evidence for an Albian Hudson arm of the North American Cretaceous Western Interior Seaway. Geol. Soc. Amer. Bull. 112, 1342–1355.

White, T.S., González, L.A., Ludvigson, G.A., Poulsen, C., 2001. The mid-Cretaceous greenhouse hydrologic cycle of North America. Geology 29, 363–366.

White, T.S., Witzke, B.J., Ludvigson, G.A., Brenner, R.L., 2005. Distinguishing base-level change and climate signals in a Cretaceous alluvial sequence. Geology 33, 13–16.

Williams, P.W., King, D.N.T., Zhao, J.-X., Collerson, K.D., 2005. Late Pleistocene to Holocene composite speleothem ^{18}O and ^{13}C chronologies from South Island, New Zealand — did a global Younger Dryas really exist? Earth Planet. Sci. Lett. 230, 301–317.

Witzke, B.J., 2003. Interpretations of North American Cretaceous dinosaur diversity trends: Society of Vertebrate Paleontologists. Abstr., J. Vertebr. Paleontol. 23 (3), 112A suppl.

Wolfe, J.A., Upchurch Jr., G.R., 1987. North American nonmarine climates and vegetation during the Late Cretaceous. Palaeogeogr. Palaeoclimatol. Palaeoecol. 61, 33–77.